Combined Solid-State NMR and Computational Approach for Probing the CO2 Binding Sites in a Porous-Organic Polymer

(Article begins on next page)

15 October 2023

iris - AperTO

Combined Solid-State NMR and Computational Approach for Probing the CO$_2$ Binding Sites in a Porous-Organic Polymer

Michele R. Chierotti,[a]* Muhamed Amin,[b] Youssef S. Hassan,[c] Rana R. Haikal,[c] Claudio Garino[a] and Mohamed H. Alkordi[c]*

[a] Department of Chemistry and NIS Centre, University of Torino, V. Giuria 7, 10125, Torino, Italy; Email: michele.chierotti@unito.it

[b] Zewail City of Science and Technology. Center for Photonics and Smart Materials, Sheikh Zayed District, 12588, Giza, Egypt.

[c] Zewail City of Science and Technology. Center for Materials Science, Sheikh Zayed District, 12588, Giza, Egypt; Email: malkordi@zewailcity.edu.eg

ABSTRACT. Herein, we report on utilization of 1D and 2D ^{13}C cross-polarization magic angle spinning (CPMAS) and MAS solid-state NMR spectroscopy in probing the binding sites and dynamical processes of ^{13}C-enriched CO_2 insides the pores of a pyridine-containing porous organic polymer (POP). Our findings from the spectroscopic measurements conducted on the evacuated sample and on the sample dosed with 800 mbar $^{13}CO_2$ indicated preferential adsorption of the CO_2 molecules at the vicinity of the basic binding sites within the POP, the pyridine rings. We further demonstrate the results of a computational study for probing the most favorable binding sites of CO_2 inside a geometrically-optimized model of the polymer in attempt to better rationalize the experimental findings from ^{13}C solid-state NMR investigations. Due to the amorphous nature of the studied POP, being also observed for a large number of emerging microporous solids, this combined approach can prove useful and versatile towards drawing a detailed picture of the gas-solid interactions, aiming for enhanced designs for futuristic materials towards CO_2 capture and sequestration.

Introduction

As novel materials are considered an essential part to advance new technologies in order to face certain socioeconomic challenges, materials that can efficiently capture, store, and/or sequester CO_2 are of great interest. Among several types of microporous solids,[1,2] conjugated microporous polymers (CMPs),[3] porous cross-linked polymers (PCPs),[4,5] and porous-organic polymers (POPs),[6] demonstrate great potentials toward this goal.[7,8] POPs constructed through non-reversible Sonogashira-Hagihara (SH)[9] cross-coupling commonly exhibit amorphous structures,[10,11] rendering their structural characterization through diffraction techniques

challenging. A myriad of structural characterization techniques that can draw more detailed picture of their chemical composition and/or connectivity include infrared, UV-Vis, solid-state NMR spectroscopy (SSNMR), X-ray photoluminescence (XPS), and energy dispersive X-ray spectroscopy (EDX), among others.[12]

However, *in situ* characterization of the material under working conditions can provide further information that is necessary to enhance our understanding of the fundamental interactions taking place inside the pores of such solids, and thus can guide rational design and syntheses strategies targeting materials with enhanced functionality. In this regards, we designed this study to probe the binding sites of CO_2 inside the pores of our previously reported pyridine-containing POP,[13] where previous investigation demonstrated favorable interactions with CO_2 due to incorporation of the basic binding sites (pyridine rings) into the backbone of the solid, Figure 1.

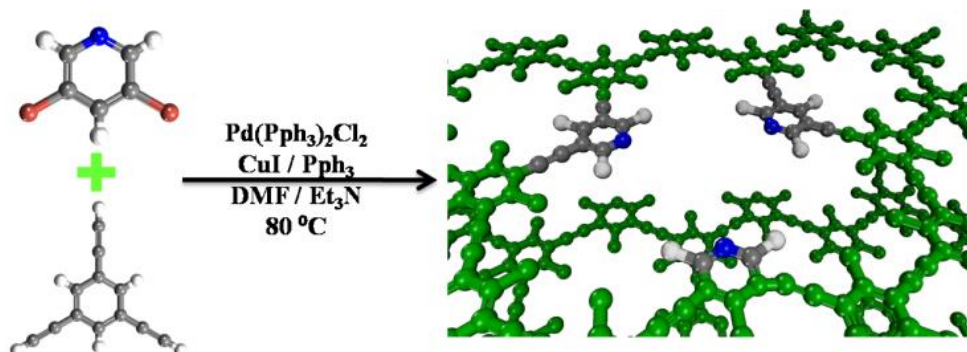**Figure 1.** Synthesis for the Pyridine POP with a structural model of a potential oligomer chain. Carbon (grey), oxygen (red), nitrogen (blue), hydrogen (white), repetitive part of the structure is shown in green.

In this report, we aim to demonstrate the abilities of SSNMR combined with *ab initio* calculation in characterizing solid-gas interactions within amorphous microporous materials for

which X-ray diffraction investigation is not possible. To the best of our knowledge, the combined experimental and theoretical approach presented here was not previously applied to such type of actively investigated microporous solids. In our setup, we utilized $^{13}CO_2$ to facilitate the experiment where $^{13}CO_2$ gas was dosed at different pressures (30 and 800 mbar) at 298 K on activated POP. In doing so, the aim was twofold: to probe the $^{13}CO_2$ adsorption sites as well as to investigate the $^{13}CO_2$ sorption dynamics within the porous structure at two extremes of $^{13}CO_2$ loading.

In this context, SSNMR is a unique technique since, depending on the type of experiment, it can either highlight signals arising from the POP structure through 1D and 2D cross-polarization (CP) experiments or the $^{13}CO_2$ signal through direct excitation experiments under static or MAS conditions. The CP experiments probe the interaction between $^{13}CO_2$ and binding sites while the direct excitation experiments focus on the $^{13}CO_2$ species within the solid and on their dynamic behavior. Several SSNMR studies were previously conducted to investigate gas adsorption in zeolites, molecular sieves, metal catalysts,[14,15] and metal-organic frameworks (MOFs)[16-19] while this approach is yet to be applied to POPs. SSNMR spectroscopy is particularly suited to this type of compounds which lack long-range order since it relies on local atomic environment.

Experimental Section

Pyridine POP was synthesized as previously reported.[10] ^{13}C-enriched (99%) CO_2 was supplied by SIAD S.p.A.

Solid-state NMR measurements. Prior to gas adsorption, the Pyridine POP sample was packed in a solid-state NMR zirconia rotors (4 mm o.d., sample volume of 80 μL) placed in a home-built quartz vacuum cell and activated under vacuum for 2h at 353 K in order to remove

adsorbed water. The complete water removing was verified through the H_2O signal disappearing in ^1H MAS spectra. After activation, the sample was contacted with increasing $^{13}CO_2$ dosages (30 and 800 mbar corresponding to 1.77 cc/g (0.08 mmol/g) and 21.5 cc/g (0.95 mmol/g) of CO_2, respectively). Then, the rotor was sealed inside the cell to avoid contact with atmospheric conditions which will result in adsorption of moisture and/or oxygen or $^{13}CO_2$ leakage.^{13}C MAS NMR spectra were acquired at the beginning and at the end of the NMR measurements to ensure the controlled atmosphere remained during MAS NMR experiments. SSNMR spectra were recorded on a Bruker Avance II 400 instrument operating at 400.23, 100.65 and 40.56MHz for ^1H, ^{13}C and ^{15}N nuclei, respectively.^{13}C MAS at 12 kHz and static spectra were acquired with the single pulse experiments (SPE) with a ^{13}C 90° pulse of 4.0 μs and recycle delays of 0.05 s (more than 5 times the longitudinal relaxation time T_1 as measured with the saturation recovery technique) for 1024 scans (MAS) or 6000 scans (static). Application of ^1H decoupling during the acquisition time resulted in no differences in the signal line shape, thus it was not applied in any MAS/static spectrum. Because of the low natural abundance of ^{13}C, the contribution to the signal from components other than the gas molecules (nearly pure $^{13}CO_2$) could be neglected.

All ^{13}C and ^{15}N CPMAS experiments employed a ramp-CP pulse sequence (^1H 90° pulse = 4 μs, relaxation delays = 3.2 s and contact times equal to 9 and 4.5 ms for ^{13}C and ^{15}N, respectively) with the TPPM ^1H decoupling with an rf field of 75 kHz during the acquisition period. 2D ^1H-^{13}C on- and off-resonance HETCOR spectra were measured with contact times of 0.1 and 7 ms, respectively, and FSLG t1 decoupling and TPPM t2 decoupling (rf fields of 82 kHz). 28 scans were averaged for 32 increments with 3.2 s of relaxation delay. The indirect ^1H chemical shift scale in the HETCOR spectra was corrected by a scaling factor of $1/\sqrt{3}$ since the ^1H chemical-shift dispersion is scaled by a factor of $1/\sqrt{3}$ during FSLG decoupling. The ^1H MAS

spectrum was acquired on Jeol ECZR 600 operating at 600.17 MHz for the ^{1}H nucleus. The

sample was packed in a 1 mm rotor (volume of 0.8 μl) and spun at 70 kHz. An echo pulse

sequence (90-τ-180-τ-acq; [1]H 90°=0.77 μs, [1]H 180°=1.54 μs) was used in order to suppress the

probe background signal. [1]H, ^{13}C and ^{15}N chemical shift scales were referenced with the

resonance of adamantane (^{1}H signal at 1.87 ppm), hexamethylbenzene (^{13}C methyl signal at 17.4

ppm) and glycine (^{15}N signal at δ=33.4 ppm with respect to NH_3) as external standards.

Computational Methods. All the calculations were performed by the Gaussian 09 program

package,[20] employing the DFT method with Grimme's B97-D functional to correct for the

dispersion forces.[21] Geometry optimization was performed employing the 6-31G(d,p) basis set.

An initial oligomeric part of the structure was optimized; starting from this optimized structure, a

CO_2 molecule was added at different starting positions and the structures were then re-optimized.

Calculations of the magnetic shielding σ were performed on the model structure (i.e. without

CO_2) and on the structure shown in Fig. 5a, using the GIAO (gauge-including atomic orbital)[22]

method at the 6-311++G(2d,2p) level. The theoretical absolute magnetic shielding (σ) values

were converted into ^{15}N chemical shifts (δ) relative to the absolute magnetic shielding of the

reference substance NH_3 (σ= 257.8ppm, δ = 0 ppm) computed at the same level.

Results and discussion

The ^{13}C CPMAS spectra with assignments for the degassed solid, and the two samples loaded

with [13]CO$_2$ under different pressures are shown in Figure 2, where the [13]CO$_2$ signal is also shown

through spectrum deconvolution. The ^{13}C CPMAS NMR spectrum of the degassed material

shows two resonances for the internal alkyne (δ = 92.0, 86.3 ppm) in agreement with the

asymmetry due to bridging pyridine and benzene rings, and two peaks for quaternary aromatic

carbons (δ = 119.8 and 122.7 ppm for benzene and pyrimidine rings, respectively). The CH benzene groups fall at 135.8 ppm, overlapped with the para-CH groups of pyridine, while the resonance at 149.6 ppm was assigned to the pyridine CH carbons in the (α) position. The spectra of the POP loaded with 30 and 800 bars differ from the degassed one only for a shoulder at 125.2 ppm attributed to the adsorbed $^{13}CO_2$ ($^{13}CO_{2(ads)}$) (Figure 3).
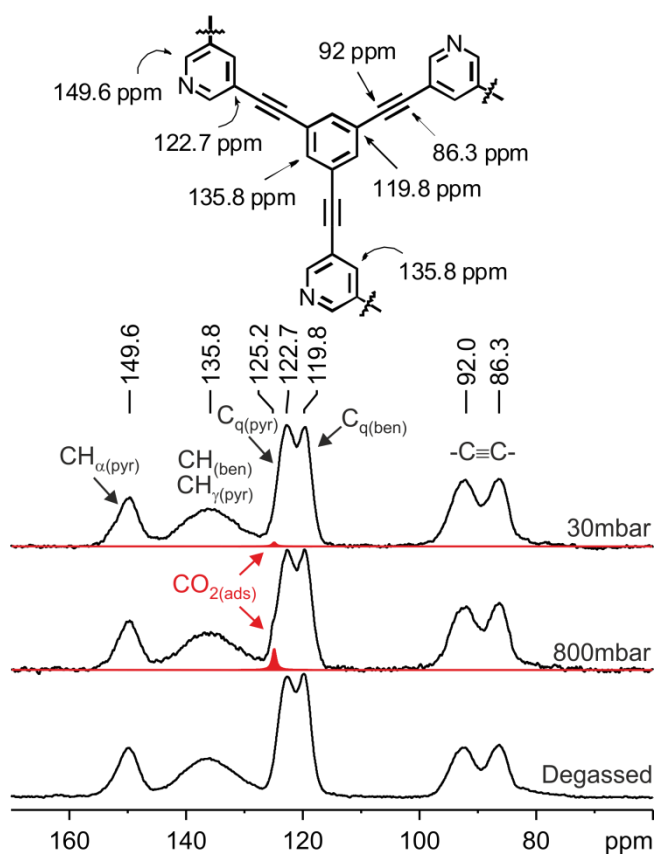

Figure 2. ^{13}C (100.65 MHz) CPMAS spectra with chemical shift and relevant assignments of (from bottom to top) degassed POP, POP loaded with 800 mbar of CO_2 and POP loaded with 30 mbar of $^{13}CO_2$ recorded at 12 kHz. In red, $CO_{2(ads)}$ signal through spectrum deconvolution.
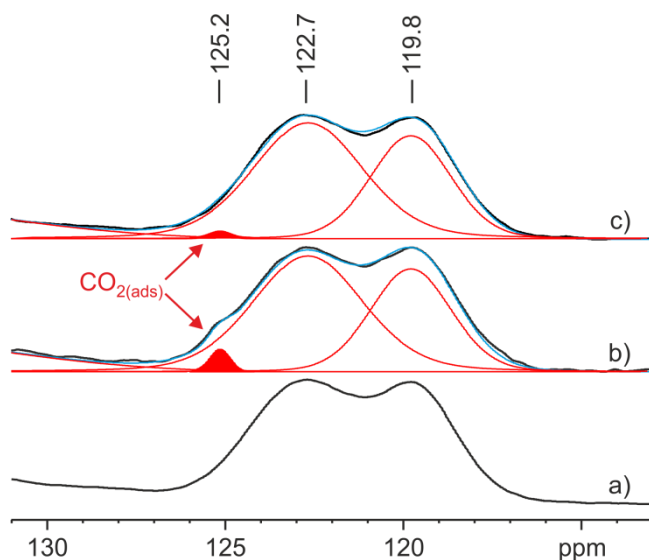
Figure 3. Aromatic region of the ^{13}C (100.65 MHz) CPMAS spectra of (a) degassed POP, (b) POP loaded with 800 mbar of CO_2 and (c) POP loaded with 30 mbar of CO_2 recorded at 12 kHz. Black lines: experimental spectra; blue lines: deconvoluted spectra; red lines: deconvoluted components.

This clearly indicates polarization transfer from the protons of the solid matrix to the adsorbed $^{13}CO_2$ molecules suggesting that the $^{13}CO_2$, although only physically adsorbed, was intimately bonded to the matrix. The peak intensity changed in accordance to the $^{13}CO_2$ pressure inside the rotor becoming barely detectable at 30 mbar. This indicated dependence of the adsorbed $^{13}CO_2$ amount on the gas pressure above the sample. This step was critical to ensure probing preferential binding sites, if any, before reaching saturation within the pores of the material. Concerning ^{15}N SSNMR data, a very small ^{15}N low-frequency shift (ca 4 ppm) was predicted by calculation for a static $CO_2\cdots N$ interaction (see the Experimental Section for further details) with respect to free pyridine nitrogen atom in agreement with the very poor polarizing ability of the

CO_2 molecule. However, due to the broad peaks observed in the experimental ^{15}N CPMAS

spectra, no significant differences can be reliably identified between the degassed sample and

that loaded with 800 bar [13]CO_2 (Figure S1 in the Supporting Information).

2D [1]H-^{13}C on- and off-resonance FSLG HETCOR spectra (Figures S2 and S3, respectively in

the Supporting Information) provided further support to our proposed scheme for [13]CO_2 binding

inside the POP since directly allow the recognition of the adsorption site. The CO_2 region of the

2D [1]H-^{13}C off-resonance FSLG HETCOR spectrum (Figure 4) shows polarization transfer from

the pyridine α protons (8.0 ppm) to the [13]CO_2 signal, as highlighted by the extracted slices

(horizontal and vertical). In addition, as shown by the peak centered around 7.8 ppm in the

column extracted at 125.2 ppm, a weaker correlation was also observed between the proton peak

at 7.4 ppm and the [13]CO_2 peak. As this ^{1}H signal was assigned to both benzene and γ pyridine

protons, it was not possible to decipher the relative significance of such two potential binding
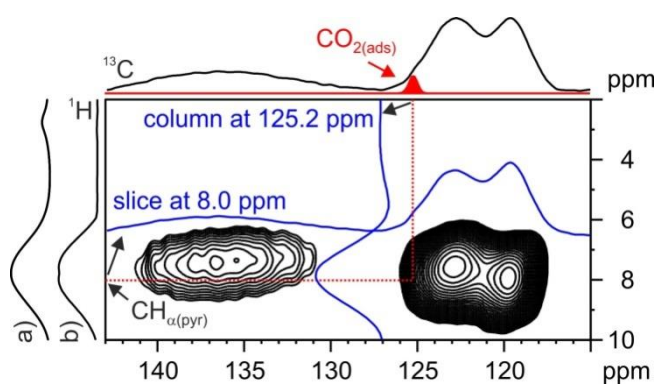
sites, based solely on the presented data.

Figure 4. CO_2 region of the [1]H-^{13}C off-resonance FSLG HETCOR spectrum of POP loaded with

800 mbar of CO_2 recorded at 12 kHz with a contact time of 7 ms. Horizontal blue line, ^{13}C slice

extracted at 8.0 ppm; vertical blue line, ^{1}H slice extracted at 125.2 ppm. In red, $CO_{2(ads)}$ signal.

(a) ^{1}H (600.17 MHz) MAS spectrum recorded at 70 kHz. (b) ^{1}H projection from the 2D spectrum.

It is reasonable to expect that the CO_2 is prevalently adsorbed on the pyridine nitrogen atoms; though it cannot be excluded that CO_2 adsorption can also occur on the bridging benzene rings. Similar information has been reported in the case of $^{13}CO_2$ adsorbed on Ag-based porous crystalline coordination polymers[23] but not yet shown for amorphous microporous solids. The off-resonance CP experiment shown in Figure 4 is set in such a way that the polarization transfer occurs only through heteronuclear dipolar interaction between the alpha H_{py} and $^{13}CO_2$ rather than through spin diffusion processes, since effectively averaged by the Lee-Goldburg conditions.[24] Due to dependence of the extent of dipolar interaction on the interatomic distance ($\propto r^{-3}$), the observed experimental correlations provided direct evidence of the $^{13}CO_2$ adsorption site(s) inside the POP.

To better understand the observations relayed by the NMR spectroscopic techniques, *ab-initio* quantum mechanical calculations were then utilized. A model composed of an oligomeric unit of the polymer was constructed and geometrically optimized using the B97-D functional to correct for the dispersion forces and the 6-31G(d,p) basis set. To this geometrically optimized model was then added a CO_2 molecule at various initial positions and the calculations rerun at the same level of theory until convergence. The calculations converged to three geometrically and energetically distinguishable structures shown in Figures 5a-c.
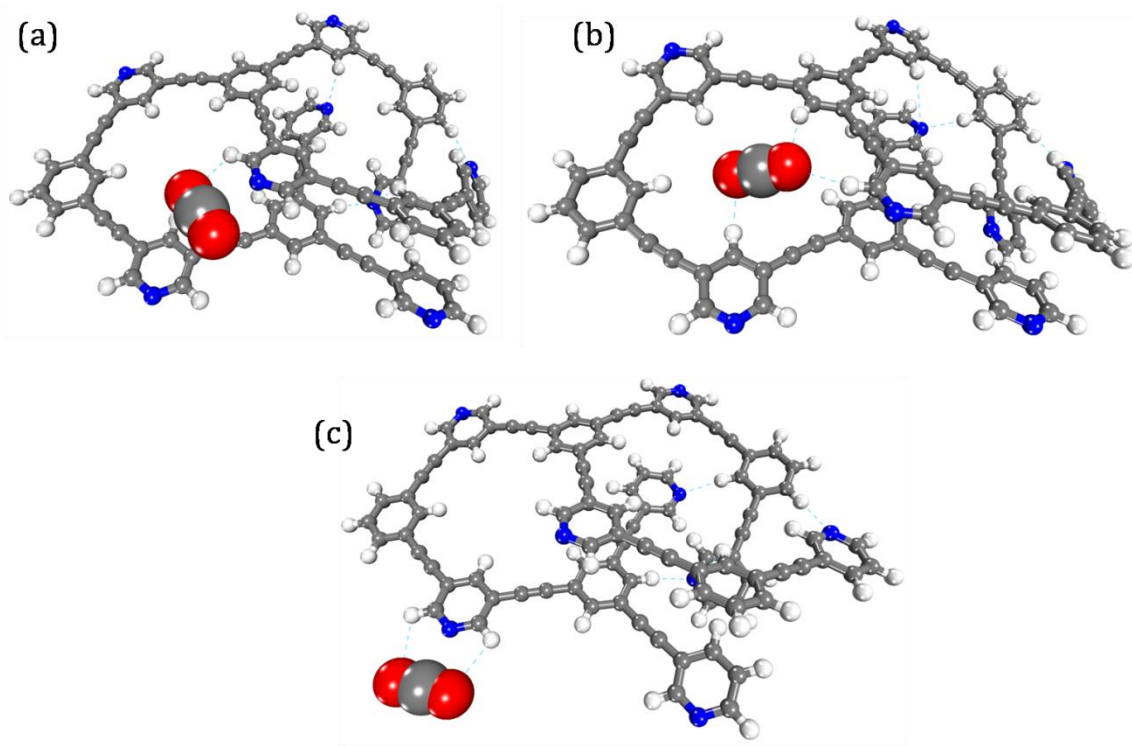
Figure 5. The B97-D/6-31G** geometrically optimized structures for the same oligomeric repeat unit and one adsorbed CO_2 molecule, showing three energetically distinct configurations with binding sites of CO_2. C (gray), O (red), N (blue), H (white), H-bonds (broken line).

The structure shown in Figure 5a demonstrated strong hydrogen bonding (H-bond) interactions between the adsorbed CO_2 molecule and a pyridine ring (through α-H atoms), D(C-H···O) = 3.359 Å, and a corresponding bond angles θ (C-H···O) = 111.517°. Additionally, this optimized structure demonstrated a strong pyridine-CO_2 binding interaction, as evidenced from short D(N···C) = 2.838 Å, in excellent agreement with that determined previously for a pyridine-CO_2 complex to be 2.7977(64) Å.[25] The structure shown in Figure 5b, displayed a CO_2 molecule with multiple bonding interactions to five H-atoms, three H-atoms from pyridine rings and two from

benzene rings. The H-bonds distances and angles were found to be $D(C-H\cdots O) = 3.556$ Å, 3.624 Å, 4.076 Å, 4.271 Å, 4.309 Å and $\theta (C-H\cdots O) = 149.085°$, 156.798°, 144.665°, 175.014°, and 173.004°, respectively. The optimized structure in Figure 5c showed a CO_2 molecule interacting with one pyridine ring, albeit a weaker interaction with slightly longer distances as compared to that in Figure 5a, $D(C-H\cdots O) = 3.457$ Å, 3.645 Å, and $\theta(C-H\cdots O) = 108.785°$ and 102.996°, respectively. The $D(N\cdots C) = 2.83$ Å is closely similar to that found in the configuration shown in Figure 5a.

It is noticed that the proposed three binding sites are in good agreement with the SSNMR results provided *vide supra*, showing correlations between CO_2 and both pyridine α-H and triethynylbenzene C-H atoms at the early adsorption stages of CO_2 (data for 30 mbar $^{13}CO_2$). The binding energy of CO_2 in the three modeled fragments was also calculated by computing the total energy of the system (CO_2 bound to the polymer) then subtracting the energy values for the optimized fragment and that for a free CO_2 molecule. The calculated binding energies for the optimized structures presented in Figures 5a-c were found to be –32.2 kJ/mol, –20.7 kJ/mol, and – 11.5 kJ/mol, respectively. These calculated values are in very good agreement with the range observed experimentally for the isosteric heat of adsorption (Q_{st}) for CO_2 in the POP, to be within the –35~ –22 kJ/mol range, Figure 6.
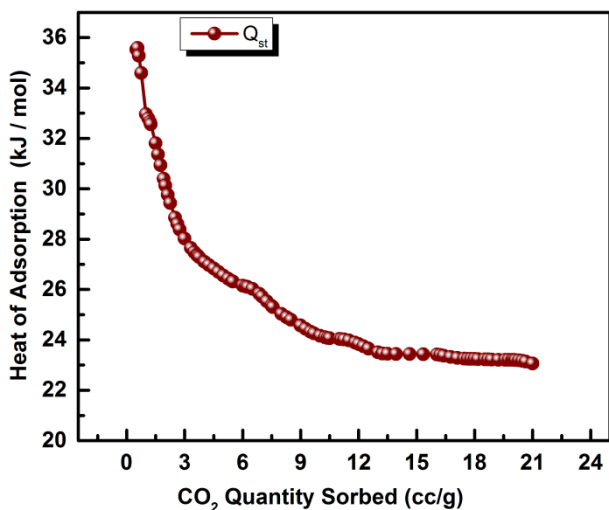
Figure 6. Isosteric heat of adsorption of CO_2 inside the POP.

To evaluate the influence of the temperature on the mobility of $^{13}CO_2$ molecules, ^{13}C MAS spectra of the samples dosed with $^{13}CO_2$ at 30 and 800 mbar were recorded at variable temperatures (293 to 353 K) and are shown in Figures 7 and 8, respectively.
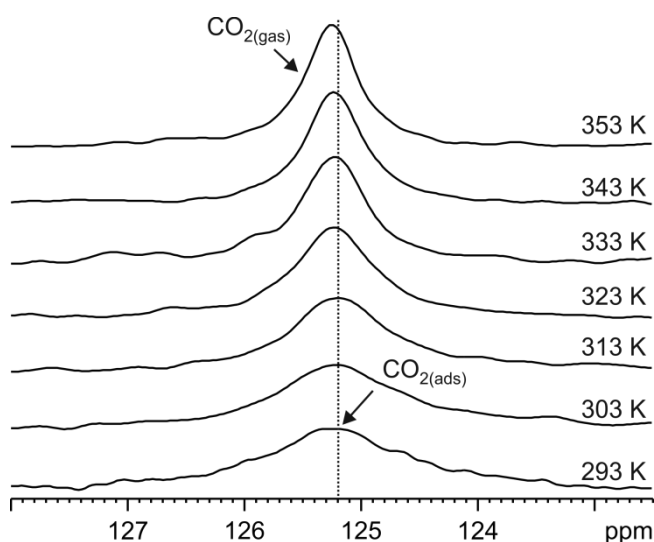

Figure 7. VT ^{13}C (100.65 MHz) MAS spectra with relevant assignments of POP loaded with 30 mbar of CO_2 recorded at a spin rate of 12 kHz, showing decreased line width upon increasing the

temperature (FWHM decreased from ~150 Hz to 55 Hz). Labels "$CO_{2(ads)}$" and "$CO_{2(gas)}$" indicate the species dominating chemical shift and shape of the signal at certain temperature.

Figure 8. VT ^{13}C (100.65 MHz) MAS spectra with relevant assignments of POP loaded with 800 mbar of CO_2 recorded at a spin rate of 12 kHz, showing decreased line width upon increasing the temperature (FWHM decreased from ~75 Hz to 25 Hz). Labels "$CO_{2(ads)}$" and "$CO_{2(gas)}$" indicate the species dominating chemical shift and shape of the signal at certain temperature.
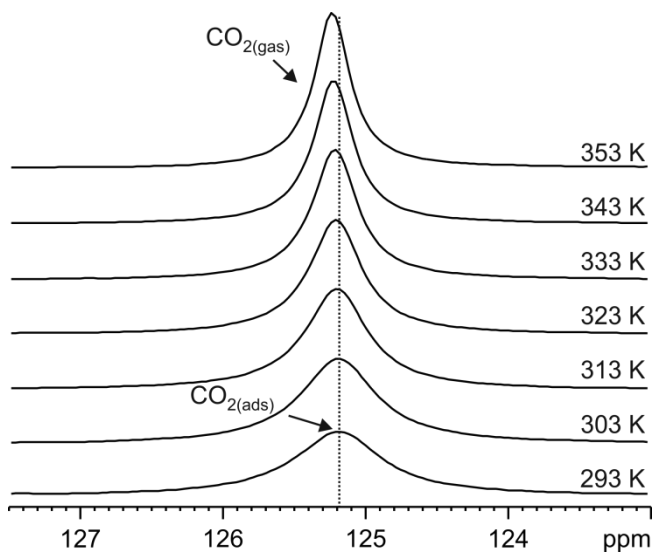
For both the low and high loading of $^{13}CO_2$, the spectra at 293 K presented a single broad resonance at 125.2 ppm, although with different line shape, FWHM of 150 Hz for the sample dosed with 30 mbar of $^{13}CO_2$, and 75 Hz for that dosed with 800 mbar. Upon increasing the temperature, the signals progressively shifted towards slightly higher frequency (up to 125.3 ppm) and became sharper (FWHM = 55 Hz and 25 Hz, respectively). Although very small, the shift was reliable and reflected the dynamic behavior of the adsorbed $^{13}CO_2$. Indeed, the small

14

shift in the peak position, and its similarity to that of $^{13}CO_2$ gas (expected at 125.3 ppm with FWHM = 30 Hz) as well as the lack, at any temperature, of a peak that can be ascribed to CO_2 gas indicated fast equilibrium among three possible $^{13}CO_2$ species: adsorbed $^{13}CO_2$, free $^{13}CO_2$ within the POP and $^{13}CO_2$ gas outside the POP (i.e. $^{13}CO_{2(ads)} \leftrightarrow {}^{13}CO_{2(POP)} \leftrightarrow {}^{13}CO_{2(gas)}$). These species appeared to be in fast exchange with each other within the NMR time scale. An analogous study on CO_2 adsorbed on UTSA-16 indicated energy barriers lower than 6 and 30 kJ·mol^{-1} for the first and second equilibrium, respectively.[16] As a consequence, peak position and line width at each temperature are probably given by the weighted average of the chemical shift and line width values between physisorbed $^{13}CO_2$ ($^{13}CO_{2(ads)}$) and free $^{13}CO_2$ co-existing in the nano-space within the POP ($^{13}CO_{2(POP)}$) and/or the free gas ($^{13}CO_{2(gas)}$).[26] The former should give rise to a very broad and shifted peak while the last two give signals more similar to that of free CO_2 gas (sharp line at 125.3 ppm). The fast equilibrium and the diamagnetic character of the POP justify the observed small shift with respect to larger values (ca. 1-3 ppm) reported for CO_2 adsorbed on MOFs, which often are paramagnetic.[27] The sharper line width for the POP loaded with 800 mbar at 293 K (FWHM ~75 Hz), compared to that of POP loaded with 30 mbar (~150 Hz), is due to the large amount of free $^{13}CO_2$ with respect to $^{13}CO_{2(ads)}$. Thus, the signal is dominated by the narrow components of $^{13}CO_{2(POP)}$ and $^{13}CO_{2(gas)}$ both experiencing a fast isotropic motion. At 30 mbar, owing to the relative higher amount of adsorbed gas, the spectrum is more dominated by $^{13}CO_{2(ads)}$, which is expected to experience an anisotropic motion or to be rigid. However, the line width is not comparable with those measured for rigid CO_2 (around 400 ppm)[28] or for CO_2 undergoing anisotropic motions (around 50 ppm),[19] implying that the binding sites have been already saturated even at the equilibrium pressure of 30 mbar i.e. a major contribution from CO_2 gas components is dominating the observed signal. At high temperature,

the amount of free CO_2 (both $^{13}CO_{2(POP)}$ and $^{13}CO_{2(gas)}$) increased thus the signals reflected the fast isotropic motion which characterizes these two species.

These observations are in good agreement with the previously measured behavior of the isosteric heat of adsorption (Q_{st}) for CO_2 inside this POP where a quick drop of Q_{st} was noticed with increased loading of CO_2, Figure 6. These observations evidenced the quick saturation of the most favored binding sites within the POP at low loading of CO_2, and thus it is reasonable to assume that the most energetically favored binding sites are those on the pyridine ring and others outlined in Figure 5.

While MAS spectra focus on the presence of equilibria among the CO_2 species, static spectra usually highlight the dynamics of the motional processes of $CO_{2(ads)}$ which can be evaluated via analysis of the signal line shapes. This has been reported for instance in the case of CO_2 adsorbed on Mg_2(dobdc).[18] The VT static ^{13}C NMR spectra of the samples loaded with 30 and 800 mbar are reported in Figures 9 and 10, respectively.
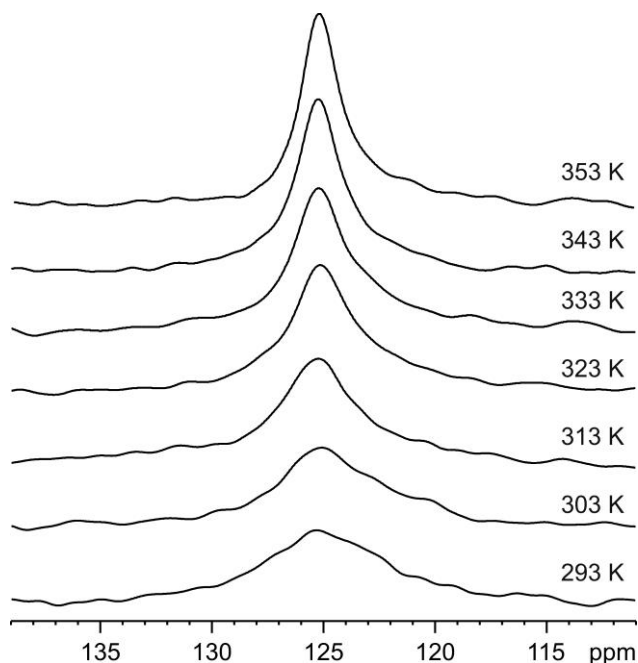
Figure 9. VT ^{13}C (100.65 MHz) static spectra of POP loaded with 30 mbar of CO_2.
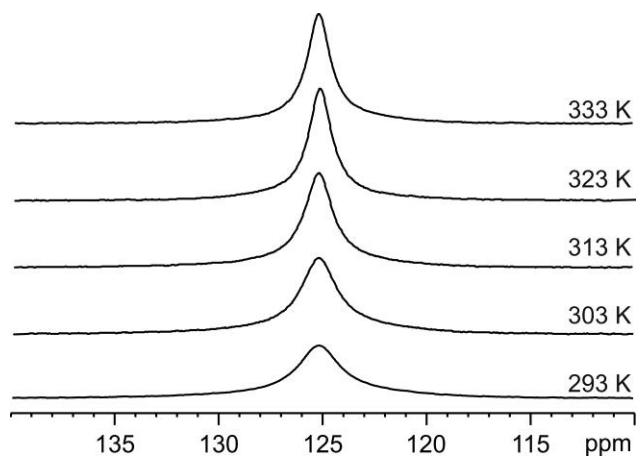

Figure 10. VT ^{13}C (100.65 MHz) static spectra of POP loaded with 800 mbar of CO_2.No further

changes are observed by increasing the temperature above 333 K.

All spectra exhibited a single peak. In the case of POP loaded with 30 mbar (Figure 9), below

313 K, the peak was quite broad (FWHM = 590 Hz) and did not present any line shape typical of

the chemical shift anisotropy (CSA) interactions. This agrees with the presence of the $^{13}CO_{2(ads)} \leftrightarrow {}^{13}CO_{2(POP)} \leftrightarrow {}^{13}CO_{2(gas)}$ equilibria with saturation of the adsorption sites already at this loading. Thus, the resulting resonance line shape is the weighted average of the expected CSA line shape due to $^{13}CO_{2(ads)}$ which is rigid or undergoing anisotropic motion and the sharp line due to $^{13}CO_{2(POP)}$ which is in fast isotropic motion.[29] By increasing the temperature to 353 K the signal narrows to 195 Hz owing to the increase of the $^{13}CO_{2(POP)}$ and $^{13}CO_{2(gas)}$ species. In the case of the POP loaded with 800 mbar of $^{13}CO_2$ (Figure 10), the signal is already very sharp (FWHM=~260 Hz) at room temperature in agreement with the higher amount of free $^{13}CO_2$ within the POP ($^{13}CO_{2(POP)}$) and $^{13}CO_2$ gas outside the POP ($^{13}CO_{2(gas)}$). A further signal sharpening was observed when the temperature was increased (FWHM ~260 Hz).

Conclusions

In conclusion, our investigations demonstrated that the most energetically favored binding site for $^{13}CO_2$ inside the POP studied here resides mostly on the nitrogen atom of the pyridine ring, and specifically in proximity of the α proton on the pyridine ring. The SSNMR techniques utilized here (mainly ^{13}C static, MAS and CPMAS, ^{15}N CPMAS and 2D ^{1}H-^{13}C off-resonance FSLG HETCOR spectra) allowed access to vital information regarding the binding sites of CO_2 inside the amorphous porous material, which are difficult to attain through other commonly utilized diffraction techniques due to the largely amorphous nature of the solid. Computational data provided a reliable confirmation of the SSNMR data adding insights on the energetic considerations of the binding sites and providing support to the observed NMR shifts. Further information on dynamic processes among CO_2 species within and outside the POP cavities are also achieved from ^{13}C static and MAS spectra. The results are discussed in terms of fast

exchange processes between physisorbed CO_2 and free CO_2 co-existing in the nano-space within the POP and/or in the outer space near the entrance.

We believe that the presented methodology can be applied to other related functional solids in order to reach better understanding of the fundamental interactions of CO_2 taking place inside the pores of certain solids; hence can aid the design for futuristic materials with desirable CO_2 capture capabilities.

Supporting Information. The following files are available free of charge: [15]N CPMAS spectra of degassed POP and POP loaded with 800 mbar of CO_2; [1]H-^{13}C on-resonance FSLG HETCOR spectrum of POP loaded with 800 mbar of CO_2, [1]H-^{13}C off-resonance FSLG HETCOR spectrum of POP loaded with 800 mbar of CO_2.

Corresponding Author

* michele.chierotti@unito.it; * malkordi@zewailcity.edu.eg

REFERENCES

1 Eddaoudi, M.; Moler, D. B.; Li, H.; Chen, B.; Reineke, T. M.; O'keeffe, M.; Yaghi, O. M., Modular Chemistry: Secondary Building Units as a Basis for the Design of Highly Porous and Robust Metal-Organic Carboxylate Frameworks. *Acc. Chem. Res.* **2001**, *34*, 319-330.

2 Orcajo, G.; Calleja, G.; Botas, J. A.; Wojtas, L.; Alkordi, M. H.; Sánchez-Sánchez, M., Rationally Designed Nitrogen-Rich Metal–Organic Cube Material: An Efficient CO_2 Adsorbent and H_2 Confiner. *Cryst. Growth Des.***2014**, *14*, 739-746.

3 Dawson, R.; Laybourn, A.; Clowes, R.; Khimyak, Y. Z.; Adams, D. J.; Cooper, A. I., Functionalized Conjugated Microporous Polymers. *Macromolecules* **2009**, *42*, 8809-8816.

4 Xie, Z.; Wang, C.; deKrafft, K. E.; Lin, W., Highly Stable and Porous Cross-Linked Polymers for Efficient Photocatalysis. *J. Am. Chem. Soc.* **2011**, *133*, 2056-2059.

5 Wang, C.; Xie, Z.; deKrafft, K. E.; Lin, W., Light-Harvesting Cross-Linked Polymers for Efficient Heterogeneous Photocatalysis. *ACS Appl. Mater. Interfaces* **2012**, *4*, 2288-2294.

6 Kaur, P.; Hupp, J. T.; Nguyen, S. T., Porous Organic Polymers in Catalysis: Opportunities and Challenges. *ACS Catal.* **2011**, *1*, 819-835.

7 Dawson, R.; Cooper, A. I.; Adams, D. J., Nanoporous Organic Polymer Networks. *Progr. Polym. Sci.* **2012**, *37*, 530-563.

8 Soliman, A. B.; Haikal, R. R.; Hassan, Y. S.; Alkordi, M. H., The Potential of a Graphene-Supported Porous-Organic Polymer (POP) for CO_2 Electrocatalytic Reduction. *Chem. Commun.* **2016**, *52*, 12032-12035.

9 Sonogashira, K.; Tohda, Y.; Hagihara, N., A Convenient Synthesis of Acetylenes: Catalytic Substitutions of Acetylenic Hydrogen with Bromoalkenes, Iodoarenes and Bromopyridines. *Tetrahedron Lett.* **1975**, *16*, 4467-4470.

10 Wu, D.; Xu, F.; Sun, B.; Fu, R.; He, H.; Matyjaszewski, K., Design and Preparation of Porous Polymers. *Chem. Rev.* **2012**, *112*, 3959-4015.

11 Haikal, R. R.; Elmansi, A. M.; Ali, P.; Hassan, Y. S.; Alkordi, M. H., One Pot Synthesis of Zr-Carboxylate Porous Hybrid Materials: Orthogonal C-C Heterocoupling and Carboxylate-Zr Assembly. *RSC Adv.* **2016**, *6*, 42307-42312.

12 Haikal, R. R.; Elmansi, A. M.; Soliman, A. B.; Aly, P.; Hassan, Y. S.; Berber, M. R.; Hafez, I. H.; Hassanien, A.; Alkordi, M. H., Tuning Surface Accessibility and Catalytic Activity of Au Nanoparticles through Immobilization within Porous-Organic Polymers. *RSC Adv.* **2016**, *6*, 94547-94555.

13 Alkordi, M. H.; Haikal, R. R.; Hassan, Y. S.; Emwas, A.-H.; Belmabkhout, Y., Poly-Functional Porous-Organic Polymers to Access Functionality - CO_2 Sorption Energetic Relationships. *J. Mater. Chem. A* **2015**, *3*, 22584-22590.

14 Sprang, T.; Boddenberg, B., Coadsorption of Xenon and Carbon Monoxide in Cadmium-Exchanged Zeolite Y Studied with ^{129}Xe NMR Spectroscopy. *J. Chem. Soc., Faraday Trans.* **1995**, *91*, 555-558.

15 Koch, M.; Brunner, E.; Pfeifer, H.; Zscherpel, D., Low-Temperature ^{13}C NMR Investigations on Carbon Monoxide Hydrogen Bonded to Brønsted Acid Sites in H Y Zeolites. *Chem. Phys. Lett.* **1994**, *228*, 501-505.

16 Masala, A.; Grifasi, F.; Atzori, C.; Vitillo, J. G.; Mino, L.; Bonino, F.; Chierotti, M. R.; Bordiga, S., CO_2 Adsorption Sites in UTSA-16: A Multi Technique Approach. *J. Phys. Chem. C* **2016**, *120*, 12068-12074.

17 Klein, N.; Herzog, C.; Sabo, M.; Senkovska, I.; Getzschmann, J.; Paasch, S.; Lohe, M. R.; Brunner, E.; Kaskel, S., Monitoring Adsorption-Induced Switching by [129]Xe NMR Spectroscopy in a New Metal–Organic Framework $Ni_2(2, 6-ndc)_2(dabco)$. *Phys. Chem. Chem. Phys.***2010**, *12*, 11778-11784.

18 Hoffmann, H. C.; Assfour, B.; Epperlein, F.; Klein, N.; Paasch, S.; Senkovska, I.; Kaskel, S.; Seifert, G.; Brunner, E., High-Pressure in Situ [129]Xe NMR Spectroscopy and Computer Simulations of Breathing Transitions in the Metal–Organic Framework $Ni_2(2, 6-ndc)_2(dabco)(DUT-8(Ni))$. *J. Am. Chem. Soc.***2011**, *133*, 8681-8690.

19 Kong, X.; Scott, E.; Ding, W.; Mason, J. A.; Long, J. R.; Reimer, J. A., CO_2 Dynamics in a Metal–Organic Framework with Open Metal Sites. *J. Am. Chem. Soc.* **2012**, *134*, 14341-14344.

20 Frisch, M. J.; Trucks, G. W.; Schlegel, H. B.; Scuseria, G. E.; Robb, M. A.; Cheeseman, J. R.; Scalmani, G.; Barone, V.; Mennucci, B.; Petersson, G. A.et al. *Gaussian 09*, Gaussian, Inc.: Wallingford, CT, USA, **2009**.

21 Grimme, S., Semiempirical GGA-Type Density Functional Constructed with a Long-Range Dispersion Correction. *J. Comput. Chem.* **2006**, *27*, 1787-1799.

22 Wolinski, K.; Hinton, J. F.; Pulay, P. Efficient implementation of the gauge-independent atomic orbital method for NMR chemical shift calculations. *J. Am. Chem. Soc.* **1990**, *112*, 8251–8260.

23 Bassanetti, I.; Comotti, A.; Sozzani, P.; Bracco, S.; Calestani, G.; Mezzadri, F.; Marchio, L., Porous Molecular Crystals by Macrocyclic Coordination Supramolecules. *J. Am. Chem. Soc.* **2014**, *136*, 14883-14895.

24 Braga, D.; Chelazzi, L.; Grepioni, F.; Dichiarante, E.; Chierotti, M. R.; Gobetto, R., Molecular Salts of Anesthetic Lidocaine with Dicarboxylic Acids: Solid-State Properties and a Combined Structural and Spectroscopic Study. *Cryst. Growth Des.* **2013**, *13*, 2564-2572.

25 Doran, J. L.; Hon, B.; Leopold, K. R., Rotational spectrum and structure of the pyridine– CO_2 van der Waals complex. *J. Mol. Struct.* **2012**, *1019*, 191-195.

26 Omi, H.; Ueda, T.; Miyakubo, K.; Eguchi T., Dynamics of CO_2 molecules confined in the micropores of solids as studied by ^{13}C NMR. *Appl. Surf. Sci.* **2005**, *252*, 660-667.

27 Hoffmann, H. C.; Debowski, M.; Müller, P.; Paasch, S.; Senkovska, I.; Kaskel, S.; Brunner, E., Solid-State NMR Spectroscopy of Metal–Organic Framework Compounds (MOFs). *Materials* **2012**, *5*, 2537-2572.

28 Gul-E-Noor, F.;Mendt, M.;Michel, D.;Pöppl, A.;Krautscheid, H.; Haase, J.; Bertmer, M., Adsorption of Small Molecules on $Cu_3(btc)_2$ and $Cu_{3-x}Zn_x(btc)_2$ Metal−Organic Frameworks (MOF) As Studied by Solid-State NMR. *J. Phys. Chem. C* **2013**, *117*, 7703-7712.

29 No significant contribution to the $^{13}CO_2$ peak line shape is expected from ^{13}C-^{13}C dipolar interactions. Indeed, although ^{13}C-enriched, for $^{13}CO_2$ gas (both $^{13}CO_{2(POP)}$ and $^{13}CO_{2(gas)}$) it is average out by rapid motion. Concerning $^{13}CO_{2(ads)}$, the molecules are too far from each other to experience a significant dipolar interaction. Indeed, the ^{13}C-^{13}C dipolar interaction is not as large as the ^{1}H-^{1}H one since it depends on γ^2 (the difference is by a factor of 16). Furthermore, it also depends on $1/r^3$ so it quickly drops by increasing the interatomic distance.

TOC Graphic